

Time-Optimal Path Planning in a Constant Wind for Uncrewed Aerial Vehicles using Dubins Set Classification

Sagar Sachdev^{*1}, Brady Moon^{*2}, Junbin Yuan¹, and Sebastian Scherer²

Abstract—Time-optimal path planning in high winds for a turning rate constrained UAV is a challenging problem to solve and is important for deployment and field operations. Previous works have used trochoidal path segments, which consist of straight and maximum-rate turn segments, as optimal extremal paths in uniform wind conditions. Current methods iterate over all candidate trochoidal trajectory types and choose the time-optimal one; however, this exhaustive search can be computationally slow. In this paper we present a method to decrease the computation time. We achieve this via a geometric approach to reduce the candidate trochoidal trajectory types by framing the problem in the air-relative frame and bounding the solution within a subset of candidate trajectories. This method reduces overall computation by 37.4% compared to pre-existing methods in Bang-Straight-Bang trajectories, freeing up computation for other onboard processes and can lead to significant total computational reductions when solving many trochoidal paths. When used within the framework of a global path planner, faster state expansions help find solutions faster or compute higher-quality paths. We also release our open-source codebase as a C++ package.

[Codebase]^a [Video]^b

Keywords: Motion and Path Planning, Aerial Systems: Perception and Autonomy, Field Robots

I. INTRODUCTION

Deploying robotic platforms in the field often necessitates taking into account additional disturbances and challenges introduced by the environment. For example, the perception could be affected by changing lighting conditions, glare, and precipitation, while the path planning and controls are affected by disturbances and changing environmental factors such as wind [1]. Ignoring these factors in path planning can lead to less robust results, suboptimal paths, infeasible paths, or even the loss of the vehicle due to collisions.

Connecting two points on a plane with a time-optimal path using a curvature-constrained motion model has been shown by [2] and proven by [3] to be a path made up of maximum curvature turns and straight segments, called a Dubins path. This solution is simple, quick to compute, and though not curvature continuous, has been applied in a variety of robotic applications such as Autonomous Underwater Vehicles (AUV) [4] and Uncrewed Aerial Vehicles (UAV)

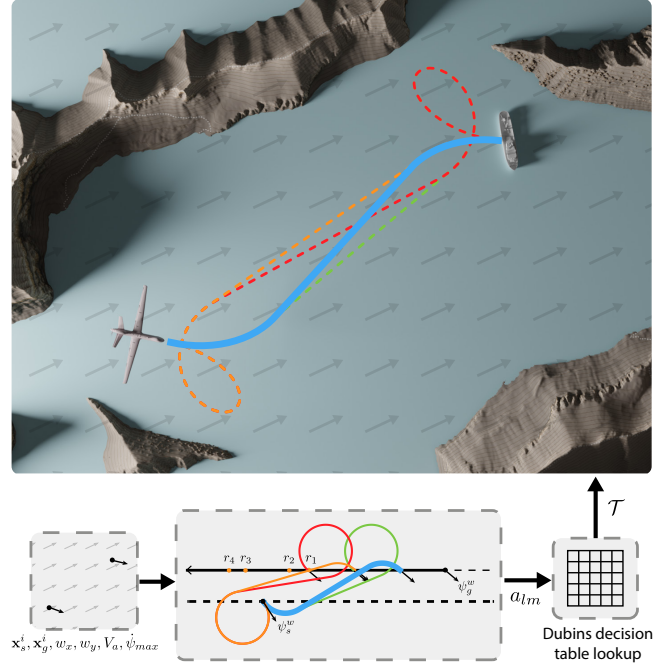


Fig. 1. An overview of our method with an example problem. The input conditions are used to find the quadrant pair for the solution to then lookup the set of candidate trajectories in the Dubins decision table. In this case, the only candidate trajectory is LSR, thus reducing the problem to solving only one out of the four potential trajectories. The bottom middle section shows the four extremal paths transformed into \mathcal{F}^w , where the goal state is moving in the negative x direction with the same speed as the wind. It is clear to see that the optimal LSR path is the first to intersect with the goal state. The upper image shows the four potential extremal paths in \mathcal{F}^i , with the blue LSR path being optimal.

[5]. However, the Dubins path does not consider the effect of wind or ocean currents on the optimal path.

This paper describes a framework for finding time-optimal curvature-constrained path planning for vehicles in a uniform flow field. We consider a kinematic model for a UAV flying at a constant altitude and constant air-relative speeds in a steady uniform wind. This research could also extend to AUVs or autonomous surface vehicles (ASVs).

This paper utilizes the framework provided by [6] to quickly compute the analytical solution for two of the four possible Bang-Straight-Bang trajectories while performing a costly global root-finding search using the Newton-Raphson method for the remaining trajectories. Iterating through solving all four trajectories and choosing the most-time optimal path is a computationally inefficient process. Through this work, we explore a solution to this problem by only needing

^{*}The first two authors contributed equally to this work.

¹Authors are with the Mechanical Engineering Department at Carnegie Mellon University, Pittsburgh, PA, USA {sagarsac, junbiny}@andrew.cmu.edu

²Authors are with the Robotics Institute, School of Computer Science at Carnegie Mellon University, Pittsburgh, PA, USA {bradm, basti}@andrew.cmu.edu

^aCodebase: <https://github.com/castacks/trochoids>

^bVideo: <https://youtu.be/qOU5gI7JshI>

to solve a subset of the possible Bang-Straight-Bang trajectories.

To reduce the number of trajectories we need to solve for, we utilize the work of [7] which identifies the optimal Bang-Straight-Bang trajectory for a Dubins path, in cases where the states are not close together, based on the distance between initial and final states as well as their angles. Through their analysis and proofs, the quadrants of the states act as a lookup in a decision table to determine the optimal trajectory type. In cases where multiple potential trajectory types exist for given initial conditions, they created switching functions to narrow down the set of trajectories to a single trajectory.

We propose a novel approach that first formulates the problem as the goal state moving at a uniform velocity in the opposite direction of the wind flow similar to [8]. We then compute the transition points where the initial or final quadrants change and find between which transition points the solution lies. Because the quadrants of the initial and final points are constant between the transition points, we can utilize the decision table presented above to predict the type of trajectory we can expect to be optimal. We then use the approach presented in [6] to compute the analytical or numerical solutions for the BSB trajectories depending on the type. This method allows us to improve overall computational efficiency and speed. This is the state-of-the-art solution, to the best of our knowledge, for computing the most time-optimal trajectories in a uniform flow field while constrained by a dynamics model. We have also released our codebase as a package for others to use, benchmark, test, and improve.

This paper is organized as follows: Section II specifies the related works, Section III outlines the problem definition, Section IV explains our methodology in depth, Section V presents our results, and Section VI gives the conclusion and future work.

II. RELATED WORK

Several approaches have been used to perform path-planning in uniform wind conditions, given some dynamic curvature constraints, namely, vehicle velocity and turning radius.

In the absence of wind conditions, the work by [7] presents an approach for planning time-optimal paths using Dubins Curves, as were first formulated by Dubins in [2]. However, instead of having to iterate over all the feasible trajectories (four in the case if the distance between the start and goal position is greater than four times the turning radius of the vehicle), they present a decision table wherein they can predict the types of feasible trajectories based on the start and goal configurations of the UAV. Based on the quadrants in which the initial orientation and the final orientation of the UAV, they can reduce the number of candidate trajectories to below four for each block of the decision table. This table produces sixteen combinations of possible quadrants, which can be represented in the form a_{lm} where l is the quadrant number of the initial and m is the quadrant number of the final orientation. A switching function then chooses

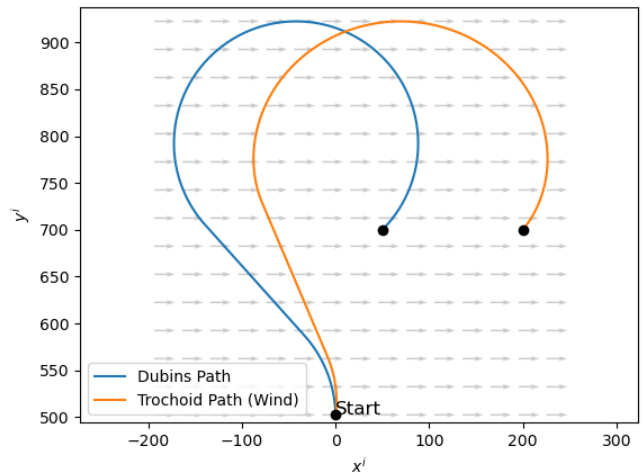


Fig. 2. An example optimal trochoidal RSL paths and its equivalent Dubins path in the wind frame.

a single trajectory from the feasible candidate trajectory in the decision table blocks. A modified version of the decision table can be found in Table I within the methodology section.

Some of the previous works have used a frame transformation to align the axis with the wind. [8] and [9] use this frame transformation to augment the problem into a moving-goal problem, wherein the velocity of the goal point is equal and opposite to the velocity of the wind. Finding intersection point is referred to as the “Rendezvous Problem.” The problem states that there are six admissible Dubins Paths, namely RSR, LSL, RSL, LSR, RLR, and LRL, wherein “R” represents a maximum turn-rate right turn, “L” represents a maximum turn-rate left turn and “S” is a Straight Line. The solutions to this problem can either be solvable or unsolvable. If the problem is solvable, the paths and their lengths can be computed for all eight admissible paths using a standard numeric root-finding approach such as the Newton-Raphson method. The path with the shortest distance is chosen as the optimal path. Fig. 2 shows a Dubins Path augmented into a trochoidal path when a wind vector is applied.

Additionally, the work by [6] also uses the same frame-alignment mentioned above. However, a key difference is that of the six admissible trajectory types, they can find closed-form solutions to two trajectory types, namely, RSR and LSL. To find the remaining four paths, it proposes using a standard numerical global root-finding approach such as Newton-Raphson. The optimal path is then found by computing the lengths of the above six paths and choosing the path with the shortest length.

Another optimal control approach was also proposed by [10] wherein it tries to solve the Markov-Dubins problem and the Zermelo’s navigation problem (which was also formulated in [9]) in order to find the shortest path to a target while avoiding obstacles and respecting the kinematic constraints of the vehicle. A key difference between the method proposed in this paper and that proposed by [9] was that this paper proposes using backward dynamic pro-

gramming to compute the optimal control policy and value function for vehicles with Dubins' type kinematics operating in the presence of wind or currents. In contrast, [9] uses the Pontryagin's maximum principle to compute the optimal control input for the kinematic airplane model.

III. PROBLEM DEFINITION

Let the system dynamics be defined by the equations

$$\begin{aligned}\dot{x}^i(t) &= V_a \cos(\psi^i(t)) + w_x \\ \dot{y}^i(t) &= V_a \sin(\psi^i(t)) + w_y \\ \dot{\psi}^i(t) &= u(t)\end{aligned}$$

where the state is given by $\mathbf{x} = [x, y, \psi]^T$, i denotes the inertial frame \mathcal{F}^i , t is time, V_a is the vehicle airspeed, w_x is the wind speed in the x axis, w_y is the wind speed in the y axis, and u is the control input.

The objective is to find the control inputs that yield the minimum time path between an initial state $\mathbf{x}_s^i = [x_s^i, y_s^i, \psi_s^i]^T$ and final state $\mathbf{x}_g^i = [x_g^i, y_g^i, \psi_g^i]^T$ given the control constraint $\|u\| < \dot{\psi}_{max}$. As was shown in [6], [8], the solution to this optimization problem is one of the six extremal paths.

IV. METHODOLOGY

On a high level, the trochoidal path planner leverages the Dubins set classification work of [7] to reduce the solutionspace of the moving goal state problem formulation of [9] and then solves the candidate solutions using the methods of [6] wherein an analytical solver is used to find the solution to the RSR and LSL trajectories and a global root finding approach is used to find the solution of the RSL and LSR trajectories. An overview of our method is outlined in Algorithm 1.

The first step is to align the x axis with the wind, transforming the frame from the inertial frame \mathcal{F}^i to the wind frame \mathcal{F}^w . The wind magnitude can be calculated at $V_w = \sqrt{v_x^2 + v_y^2}$, and the angle, ψ_w , can thus be computed as

$$\psi_w^i = \tan^{-1} \left(\frac{v_y}{v_x} \right) \quad (1)$$

Let ψ_s^w and ψ_g^w be the wind start and goal angles defined as

$$\psi_s^w = \psi_s^i - \psi_w^i \quad (2)$$

$$\psi_g^w = \psi_g^i - \psi_w^i \quad (3)$$

The x and y elements of the start and goal states are transformed from \mathcal{F}^i to \mathcal{F}^w with the rotational matrix

$$R_i^w = \begin{bmatrix} \cos(\psi_w^i) & \sin(\psi_w^i) \\ -\sin(\psi_w^i) & \cos(\psi_w^i) \end{bmatrix} \quad (4)$$

The problem can now be viewed as finding the minimum time intersection point of the vehicle and goals state, with the wind being removed from the vehicle system dynamics and viewing the goals state as moving in the negative x direction

Algorithm 1: Trochoid($\mathbf{x}_s^i, \mathbf{x}_g^i, w_x, w_y, V_a, \dot{\psi}_{max}$)

```

1 Set  $\mathbf{x}_s^w, \mathbf{x}_g^w$  using (1-4);
2  $\Gamma \leftarrow \emptyset$ ;
3  $\delta\theta_\alpha \leftarrow \text{CalcDeltaTheta}(\psi_s^w)$ ;
4  $\delta\theta_\beta \leftarrow \text{CalcDeltaTheta}(\psi_g^w)$ ;
5  $\Gamma \leftarrow \{\text{CalcTransitionPoints}(\psi_s^w, \delta\theta_\alpha)\}$ ;
6  $\Gamma \leftarrow \Gamma \cup \{\text{CalcTransitionPoints}(\psi_g^w, \delta\theta_\beta)\}$ ;
7 for  $r_n \in \Gamma$  do
8   if  $\text{CheckSegment4R}(r_n)$  then
9      $\mathcal{T} \leftarrow \{\text{RSR}, \text{RSL}, \text{LSL}, \text{LSR}\}$ ;
10    break;
11    $l_p \leftarrow \text{DubinsPath}(r_n)$ ;
12    $t_{start} = l_p/V_a; t_{goal} = r_n/V_w$ ;
13   if  $t_{start} \leq t_{goal}$  then
14     Compute  $\theta_q$  using (6);
15     break;
16 if  $\theta_q$  is empty then
17   Compute  $\theta_q$  as angle between  $r_N$  and  $\pi$ ;
18    $\alpha_q = \psi_s^w - \theta_q; \beta_q = \psi_g^w - \theta_q$ ;
19    $a_{lm} \leftarrow \text{FindQuadrants}(\alpha_q, \beta_q)$ ;
20    $\mathcal{T} \leftarrow \text{DecisionTable}(a_{lm})$ ;
21 for each candidate trochoidal trajectory in  $\mathcal{T}$  do
22   Solve for  $u$  using (7-21);
23   if  $\text{PathTime}(u) < \text{PathTime}(u_{best})$  then
24      $u_{best} \leftarrow u$ 
25 return  $u_{best}$ 

```

with the velocity V_w . The updated system dynamics of the vehicle would be

$$\begin{aligned}\dot{x}^w(t) &= V_a \cos(\psi^w(t)) \\ \dot{y}^w(t) &= V_a \sin(\psi^w(t)) \\ \dot{\psi}^w(t) &= u(t)\end{aligned}$$

and the goal state position at time t would be

$$\begin{aligned}\mathbf{x}_g^w(t) &= \mathbf{x}_g^w - tV_w \\ y_g^w(t) &= y_g^w \\ \psi_g^w(t) &= \psi_g^w\end{aligned}$$

With the problem formulated in this manner, connecting any two *static* points in \mathcal{F}^w can be treated as a Dubins problem, as there is no wind acting on the vehicle. A Dubins path can be solved with just the distance between the two states and the orientation of the start and goal states relative to the axis connecting the two states. We define this axis-aligned frame as \mathcal{F}^d shown in Fig. 3. To find the Dubins path between the static start state and a goal state parameterized by a given t , the angles ψ_s^w and ψ_g^w are transformed to the Dubins frame, \mathcal{F}^d by first computing the angle, θ , between the two points with

$$\theta(t) = \tan^{-1} \left(\frac{y_g^w(t) - y_s^w}{x_g^w(t) - x_s^w} \right)$$

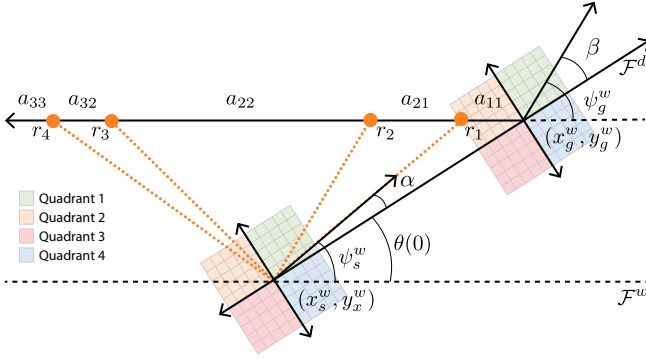


Fig. 3. An example problem setup with variable definition shown. In this example, there are four transition points which is the maximum. Depending on V_a , w_x , w_y , and ψ_{max} , the solution would lie within one of the quadrant pair sections.

The initial and the final angles in \mathcal{F}^d , α and β , can be computed as

$$\begin{aligned}\alpha(t) &= \psi_s^w - \theta(t) \\ \beta(t) &= \psi_g^w - \theta(t)\end{aligned}$$

With α , β , and the distance d between the states, the Dubins path between the states can be found. If $d > 4R$, where R is the turning radius, we can directly look up the optimal extremal path type based on the quadrants of α and β [7]. Taking the length of this path, the time of traversal for the vehicle would be $t_{start} = l_p/V_a$ where l_p is the length of the path. The time for the goal state to reach the state at the speed of V_w would be $t_{goal} = t$. If t_{start} is equal to t_{goal} , then this would be the rendezvous time and state.

As the goal-point moves in the direction opposite to the wind, the θ changes along with both $\alpha(t)$ and $\beta(t)$. We can divide the goal state trajectory into sections based on the points along the trajectory where $\alpha(t)$ or $\beta(t)$ transitions into new quadrants. Each section defines a period where the quadrants of $\alpha(t)$ and $\beta(t)$ are constant. If we can find which section of the path contains the solution, we can constrain the solution space based on the quadrants of $\alpha(t)$ and $\beta(t)$.

Proposition 1: If the solution lies between the transition points r_n and r_{n-1} , then the set of candidate optimal trajectories \mathcal{T} is the block in the Dubins decision table associated with any α or β angle derived from a point between r_n and r_{n-1} .

Proof: Let the quadrant of α be l , the quadrant of β be m , and the quadrant pair a_{lm} denotes the block of row l and column m in the Dubins decision table. Any transition point r_n denotes a change of l or m . Therefore between r_n and r_{n-1} , l and m stay constant. Therefore a_{lm} is the same for all α and β between the transition points. Any of such values can be used to find a_{lm} and the corresponding set of candidate optimal trajectories \mathcal{T} from the block in the decision table. ■

We define the point where $\alpha(t)$ or $\beta(t)$ transitions to a new quadrant as r_n , where $n \in N$, N is the total number of transition points, and Γ is the ordered set of transition points.

The first quadrant transition for $\alpha(t)$ is at $\theta_{\alpha 1} = \delta\theta_\alpha + \theta(0)$ where $\delta\theta_\alpha$ is the rotation for $\alpha(t)$ to transition to a new quadrant and is positive when y_g^w is positive and negative when y_g^w is negative. This is due to $\theta(t)$ rotating in the positive direction when the goal state $\mathbf{x}_g^w(0)$ is above the start state \mathbf{x}_s^w and rotating in the negative direction when the goal state is below the start state.

If the rotation from $\theta(0)$ to $\theta_{\alpha 1}$ doesn't cross the x axis, then the transition point can be computed by

$$r_n = x_g^w - x_s^w - \frac{y_g^w - y_s^w}{\tan(\theta_{\alpha 1})} \quad (5)$$

which is the distance from $\mathbf{x}_g^w(0)$ where $\mathbf{x}_g^w(t)$ intersects with the line from \mathbf{x}_s^w in the $\theta_{\alpha 1}$ direction. There is no intersection point if $\theta_{\alpha 1}$ is directed away from the goal state trajectory.

The following transition point angle $\theta_{\alpha 2}$ is $\frac{\pi}{2}$ from $\theta_{\alpha 1}$ in the same direction as $\delta\theta_\alpha$. Just as before, if $\theta_{\alpha 2}$ does not cross the x axis, then the next transition point is calculated with (5) using $\theta_{\alpha 2}$. This process is then repeated for $\beta(t)$ to find its transition points. An example configuration can be seen in Fig. 3. There can be at most 4 total transition points, as a rotation of $\frac{\pi}{2}$ from either of the latter points would lead to an angle pointing away from the goal state trajectory.

The transition points are then iterated over to check if the solution lies before that point. First, the segment between the transition point and the previous one is checked to satisfy the $d > 4R$ condition. If the check is satisfied, the time it takes to go from the goal state to the transition point r_n is computed by $t_{goal} = r_n/V_w$. Similarly, the time for the vehicle to travel from the start state to the transition point is also computed by finding the Dubins path between the points and then solving for the time with $t_{start} = l_p/v$, where l_p is the path length. If $t_{start} < t_{goal}$, it means that the solution lies between the transition points. To find the quadrants for the section, we compute the angle of the midpoint between the transition points with

$$\theta_q = \tan^{-1} \left(\frac{y_g - y_s}{x_g - x_s - \frac{r_n + r_{n-1}}{2}} \right) \quad (6)$$

Using the midpoint rather than the transition point ensures that the lookup of the quadrants does not lie on a boundary.

If the solution does not lie between any of the transition points ($t_{start} > t_{goal}$ for all transition points), then the solution lies beyond the last transition point. If that happens, rather than computing the angle of the midpoint between transition points, we directly compute the θ_q as halfway between the last transition point and π .

After finding θ_q , the associated initial and final angles α_f and the β_f are found using the following equation:

$$\begin{aligned}\alpha_q &= \psi_s^w - \theta_q \\ \beta_q &= \psi_g^w - \theta_q\end{aligned}$$

We can then find the quadrant l of α_q and the quadrant m of β_q , creating the pair a_{lm} . We check the corresponding block in the Dubins decision table and let \mathcal{T} represent the set of candidate trajectories within that block.

$Q_g \backslash Q_s$	1	2	3	4
1	RSL	RSR RSL LSR	RSR LSR	LSR RSL RSR
2	LSL RSL LSR	LSL RSL RSR	RSR	RSR RSL
3	LSL LSR	LSL	RSR LSR LSL	RSR LSR RSL
4	RSL LSR LSL	LSL RSL	LSL LSR RSL	LSR

TABLE I. The above Dubins decision table is adapted from [7] with corrections to $\{a_{12}, a_{21}, a_{34}, a_{43}\}$. “R” represents a right-turn segment, “S” represents a straight segment, and “L” represents a left-turn segment. Q_s is the quadrant of the start state, and Q_g is the quadrant of the goal state.

During the implementation and testing of the Dubins decision table based on [7], inconsistencies between the decision table and result were seen, particularly in the no-wind cases. This error was validated by computing and comparing all six admissible paths in the Dubins set. We found that the decision table sometimes does not give the actual shortest path for quadrant pair $a_{lm} \in \{a_{12}, a_{21}, a_{34}, a_{43}\}$. These four cases are equivalent with symmetry, and we describe the issue in detail within the Appendix. A corrected version of the Dubins decision table is also provided in Table I.

After finding \mathcal{T} , we solve the trochoid paths within the set using the method described in [6] and choose the one within minimum time, but we now no longer have to iterate over all candidate solutions in most cases. As seen in Table I, all blocks have less than four path types, with some having only one. Only when the solution is less than $4R$ do all path types have to be checked.

For paths of type RSR or LSL, the solutions can be found analytically using the values

$$x_{s0} = x_s^w - \frac{V_a}{\delta_1 \omega \sin(\psi_s^w)} \quad (7)$$

$$y_{s0} = y_s^w + \frac{V_a}{\delta_1 \omega \cos(\psi_s^w)} \quad (8)$$

$$x_{g0} = x_g^w - \frac{V_a}{\delta_2 \omega \sin(\delta_2 \omega t_{2\pi}) + \psi_g^w} - V_w t_{2\pi} \quad (9)$$

$$y_{g0} = y_g^w + \frac{V_a}{\delta_2 \omega \cos(\delta_2 \omega t_{2\pi}) + \psi_g^w} \quad (10)$$

and the point of exit of the first bank t_1 and the point of entry to the second bank t_2 for LSL and RSR trajectories

can be found with

$$\gamma = \tan^{-1} \left(\frac{y_{g0} - y_{s0}}{x_{g0} - x_{s0} + V_w \frac{\psi_s^w - \psi_g^w + 2k\pi}{\delta_2 \omega}} \right) \quad (11)$$

$$t_1 = \frac{t_{2\pi}}{\delta_1 2\pi} \left(\sin^{-1} \left(\frac{V_w}{V_a} \sin(\gamma) \right) + \gamma - \psi_s^w \right) \quad (12)$$

$$t_2 = t_1 + \frac{\psi_s^w - \psi_g^w + 2k\pi}{\delta_2 \omega},$$

$$k \in \{-3, -2, -1, 0, 1, 2\} \quad (13)$$

where $\delta_1 \in \{-1, 1\}$ and $\delta_2 \in \{-1, 1\}$ result in a left or right turn for the first and second bank, $\omega = |\dot{\psi}_{max}|$, $t_{2\pi} = 2\pi/\omega$, and $\psi_s^w - \psi_g^w$ is modulo 2π .

If the solution is of RSL or LSR, they can be found using a numerical root-finding technique such as the Newton-Raphson solver to find the roots of the equation

$$f(t_1) = E \cos(\delta_1 \omega t_1 + \psi_s^w) + F \sin(\delta_1 \omega t_1 + \psi_s^w) - G \quad (14)$$

where,

$$E = V_a \left(V_w \frac{\delta_1 - \delta_2}{\delta_1 \delta_2 \omega} - (y_{g0} - y_{s0}) \right) \quad (15)$$

$$F = V_a \left(x_{g0} - x_{s0} + V_w \left(t_1 \left(\frac{\delta_1}{\delta_2} - 1 \right) + \frac{\psi_s^w - \psi_g^w + 2k\pi}{\delta_2 \omega} \right) \right) \quad (16)$$

$$G = V_w (y_{g0} - y_{s0}) + \frac{V_a^2 (\delta_2 - \delta_1)}{\delta_1 \delta_2 \omega} \quad (17)$$

and then using t_1 to find t_2 using (13). Because there are multiple solutions, each has to be checked to find the optimal trajectory.

After finding t_1 and t_2 , the trochoidal paths can be constructed using

$$x_s^w(t) = \frac{V_a}{\delta_1 \omega} \sin(\delta_1 \omega t + \psi_s^w) + V_w t + x_{s0} \quad (18)$$

$$y_s^w(t) = \frac{V_a}{\delta_1 \omega} \cos(\delta_1 \omega t + \psi_s^w) + y_{s0} \quad (19)$$

$$x_g^w(t) = \frac{V_a}{\delta_2 \omega} \sin(\delta_2 \omega t + \psi_g^w) + V_w t + x_{g0} \quad (20)$$

$$y_g^w(t) = \frac{-V_a}{\delta_2 \omega} \cos(\delta_2 \omega t + \psi_g^w) + y_{g0} \quad (21)$$

where $t \in [0, t_1]$ for the first two equations to construct the first banking segment, and $t \in [t_2, t_{2\pi}]$ for the last two equations to construct the second banking segment. For derivations of (7-21) and more in-depth explanations, see [6].

The C++ package for our method is found at <https://github.com/castacks/trochoids>. The README contains instructions for how to build, run, and test the codebase. Since the target application for this planner is UAVs, we also wanted to be able to handle changes in altitude between start and goal states. To do this we simply added a linear interpolation of the altitude between the start and goals states for all points in the path. Other methods could include only changing altitude on the straight segment or adding helical paths at the end or beginning to climb or descend.

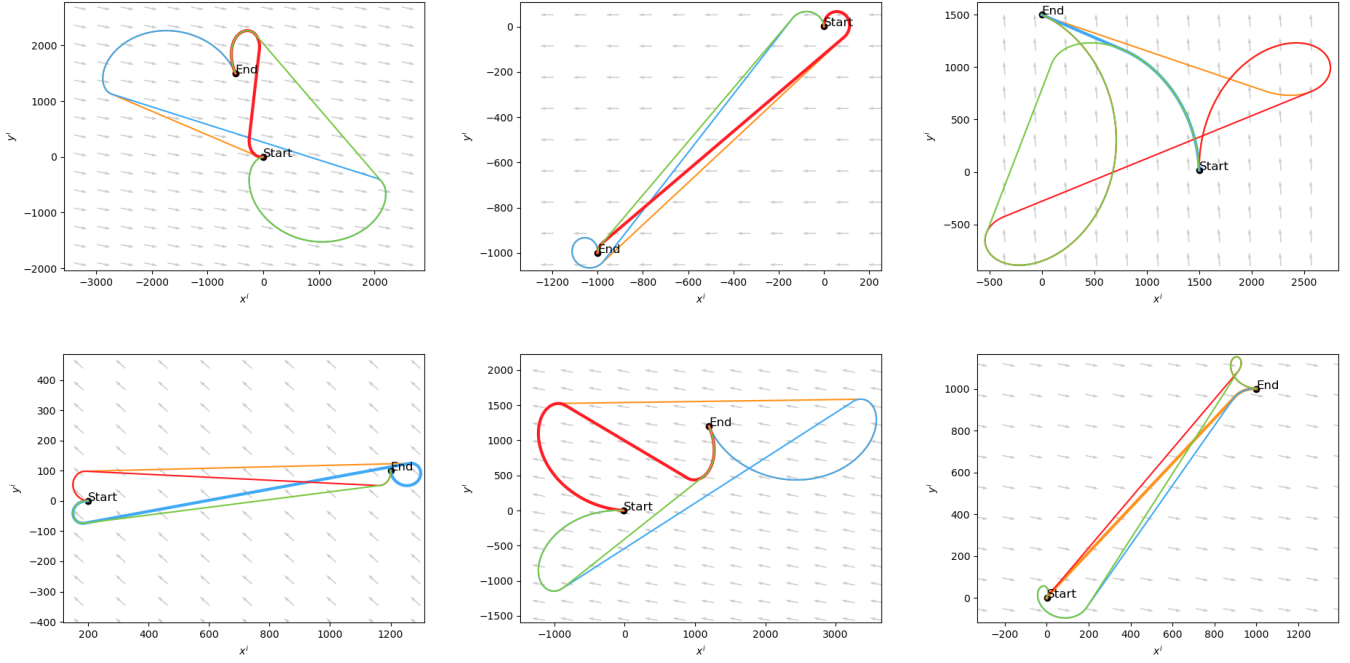


Fig. 4. Randomly sampled candidate BSB trajectories for randomly selected initial and final states in a uniform wind-vector field. RSL is shown as red, RSR as orange, LSL as green, and LSR as blue. The bolded path in each subfigure is the optimal one.

V. TESTING RESULTS

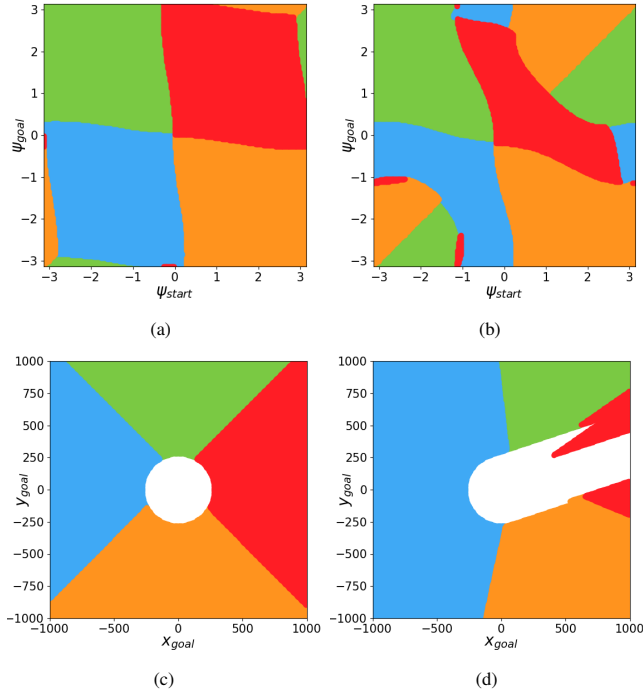


Fig. 5. The first two figures show the distribution of solutions across varying ψ_s^i and ψ_g^i values and illustrate the difference between cases with wind speed zero (5a) and with wind speed 12.65 m/s (5b). The last two figures show the distribution of the solutions across varying start and goal states with wind speed zero (5c) and wind speed 12.65 m/s (5d). RSL is shown as red, RSR as orange, LSL as green, and LSR as blue.

We validate our proposed method by performing Monte-Carlo simulations. The start and goal poses x_s^i , y_s^i , x_g^i and y_g^i were randomly sampled from a uniform distribution in the range $[-1000, 1000]$. Similarly, ψ_s^i , ψ_g^i , and ψ_w^i were uniformly sampled in the range $[0, 2\pi]$. Additionally, the wind speed V_w was randomly sampled in the range $[1, 15]$ m/s, and the turning radius R_0 was sampled in the range $[10, 1000]$ m. The UAV airspeed was set as $V_a = 20$ m/s throughout all tests. Fig. 4 shows six randomly sampled trajectories.

The average run-time over 10,000 sampled parameters for Bang-Straight-Bang trajectories on a 3.40 GHz CPU was 1.4224 ms with a standard deviation of 8.006×10^{-5} ms as compared to the baseline method, where two analytical solves and two numerical solves were iterated over, and the shortest path length selected [6]. This baseline method had an average solve time of 2.2711 ms with a standard deviation of 2.97077×10^{-5} ms. The testing results yielded a 37.4% improvement over the baseline method, and the P value for the single tail difference between the two means is well less than 0.0001. We found that 91.73% of the 10,000 cases satisfy the $d > 4R_0$ condition mentioned in Section IV, which determines the optimal trajectories are of type Bang-Straight-Bang.

Table II shows the distribution of the Bang-Straight-Bang trajectories for the 10,000 runs, and the optimal candidate trajectory types are evenly spread out at approximately 25%. The distribution for the quadrant pairs of the tests within the Dubins decision table can be seen in Table III. The

Path Type	Distribution
LSL	25.8%
LSR	24.88%
RSL	24.6%
RSR	24.68%

TABLE II. The distribution of time-optimal path types based on Monte-Carlo simulations for Bang-Straight-Bang trajectories.

Decision table block	Distribution
a_{11}	5.26%
a_{12}	5.48%
a_{13}	5.46%
a_{14}	4.96%
a_{21}	5.51%
a_{22}	5.40%
a_{23}	5.44%
a_{24}	5.30%
a_{31}	5.99%
a_{32}	5.37%
a_{33}	5.78%
a_{34}	5.72%
a_{41}	5.54%
a_{42}	5.79%
a_{43}	5.16%
a_{44}	5.32%

TABLE III. The distribution of Dubins decision table blocks from the Monte-Carlo simulations.

overall distribution of trajectories within a specific block for the 10,000 randomly sampled cases was also somewhat equivalent, showing full coverage of the testing domain.

We also visualize and compare the distributions of the optimal trajectory types for Dubins and trochoidal paths over various conditions in Fig. 5. For these figures, $V_a = 20$ m/s, $V_w = 12.65$ m/s, $\psi_w = 0.322$ rad, and $R_0 = 70$ m. Fig. 5a shows the optimal Dubins trajectories, where the wind is ignored, for $x_s^i = 0$, $y_s^i = 0$, $x_g^i = 470$ and $y_g^i = 0$, and the initial and goal angles ψ_s^i and ψ_g^i are sampled from $[-\pi, \pi]$. The distribution of the trajectory types for wind cases can be seen in Fig. 5b, depicting a shift in the decision boundaries for the wind cases. Similarly, start and goal angles were held constant at $\psi_s^i = \pi/4$ and $\psi_g^i = 3\pi/4$ and the start and goal positions were sampled from a range of $[-1000, 1000]$ m with the same R_0 and V_w as mentioned above. The distribution for Dubins trajectories (ignoring the wind) can be seen in Fig. 5c, whereas the distribution of trochoidal trajectories can be seen in Fig. 5d. The white hole in the center indicates states that do not satisfy the $d > 4R_0$ condition and thus have not been included in the plot. The shift in trajectory type distributions from the effects of wind shows why the same switching functions from [7] cannot be used directly for choosing the optimal trajectories.

To validate the robustness of this approach, we tested 5 million randomly sampled start states, goal states, wind speeds, and turning radii and compared the trajectory outputs to the numerical solution as well as the analytical solution when available. Through this rigorous testing, we found the aforementioned error in the Dubins decision table, which occurred in only 3 out of a million test cases. Fixing this error necessitated adding an additional numerical solve to

four quadrant pair cells. Adding these extra numerical solves affected the bounds of the maximum time improvements of our method. With the baseline having two numerical solves for every solution, we were initially able to reduce the average number of numerical solves to 1 using the original decision table, achieving approximately a 50% improvement from the baseline. However, to make this approach more robust, fixing the error in the decision table caused the average number of numerical solves to increase to 1.25, giving a maximum theoretical speed reduction of 37.5%.

VI. CONCLUSION

Based on the extensive testing results, the proposed method to compute time-optimal paths for curvature-constrained vehicles in a uniform wind outperforms baseline methods. The proposed approach reduces computation time, which is particularly important for real-time autonomous navigation systems such as UAVs, AUVs, or ASVs, especially in scenarios with limited computational capacities onboard. The future direction of this work is to explore fully implementing the switching functions for each quadrant block in the decision table rather than iterating over the potential trajectories in each cell, computing the lengths of the trajectories, and choosing the shortest one.

ACKNOWLEDGMENT

This work is supported by the Office of Naval Research (Grant N00014-21-1-2110). This material is based upon work supported by the National Science Foundation Graduate Research Fellowship under Grant No. DGE1745016.

Thank you to Oswaldo Ramirez for his help on the video and proofreads.

REFERENCES

- [1] M. Kulkarni, B. Moon, K. Alexis, and S. Scherer, *Aerial Field Robotics*, pp. 1–15. Berlin, Heidelberg: Springer Berlin Heidelberg, 2020.
- [2] L. E. Dubins, “On curves of minimal length with a constraint on average curvature, and with prescribed initial and terminal positions and tangents,” *American Journal of Mathematics*, vol. 79, no. 3, pp. 497–516, 1957.
- [3] H. H. Johnson, “An application of the maximum principle to the geometry of plane curves,” *Proceedings of the American Mathematical Society*, vol. 44, no. 2, pp. 432–435, 1974.
- [4] Y. Wang, W. Cai, and Y. R. Zheng, “Dubins curves for 3d multi-vehicle path planning using spline interpolation,” in *OCEANS 2017 - Anchorage*, pp. 1–5, 2017.
- [5] M. Owen, R. W. Beard, and T. W. McLain, *Implementing Dubins Airplane Paths on Fixed-Wing UAVs**, pp. 1677–1701. Dordrecht: Springer Netherlands, 2015.
- [6] L. Techy and C. A. Woolsey, “Minimum-time path planning for unmanned aerial vehicles in steady uniform winds,” *Journal of Guidance, Control, and Dynamics*, vol. 32, no. 6, pp. 1736–1746, 2009.
- [7] A. M. Shkel and V. Lumelsky, “Classification of the dubins set.” *Robotics and Autonomous Systems*, vol. 34, no. 4, pp. 179–202, 2001.
- [8] T. McGee, S. Spry, and J. Hedrick, “Optimal path planning in a constant wind with a bounded turning rate,” *Collection of Technical Papers - AIAA Guidance, Navigation, and Control Conference*, vol. 5, 08 2005.
- [9] T. G. McGee and J. K. Hedrick, “Optimal path planning with a kinematic airplane model,” *Journal of Guidance, Control, and Dynamics*, vol. 30, no. 2, pp. 629–633, 2007.
- [10] E. Bakolas and P. Tsiotras, “Time-optimal synthesis for the zermelo-markov-dubins problem: The constant wind case,” in *Proceedings of the 2010 American Control Conference*, pp. 6163–6168, 2010.

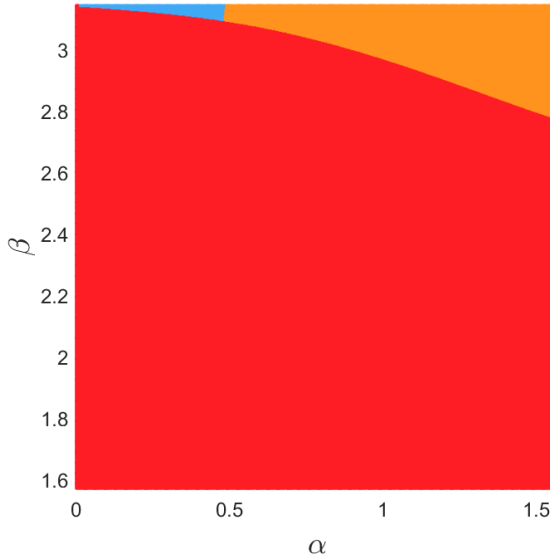


Fig. 6. The shortest path distribution for case a_{12} with $\alpha \in [0, \pi/2]$ and $\beta \in [\pi/2, \pi]$ with $d = 4.01R_0$. The red region marks the quadrant pairs for which the shortest path is **RSL**. The orange region marks the quadrant pairs for which the shortest path is **RSR** and the blue region marks the quadrant pairs for which the shortest path is **LSR**.

APPENDIX

In [7], a decision table is proposed to compute the shortest feasible path among the Dubins set $D = \{LSL, RSR, RSL, LSR, RLR, LRL\}$, given the quadrants of α and β . After implementing and validating each block within this table, 4 cases were found, $a_{lm} \in \{a_{12}, a_{21}, a_{34}, a_{43}\}$, where the previously proposed table did not give the actual shortest path option. Symmetrically, these 4 cases are equivalent. As such, the specific case of block a_{12} , which starts in quadrant 1 and finishes in quadrant 2, is addressed below.

According to the proposition 9 in [7], the shortest path for a_{12} is either RSR or RSL based on the results of the switching function S_{12} . However, after comprehensive testing, there are cases where the shortest path is LSR. This is particularly evident when the departing angle α is close to 0 and the arriving angle β is close to π . This was overlooked in the proof of proposition 9 based on the differential analysis in the neighborhood of the edge case.

To visualize the solution space, we sampled across α and β for a_{12} with $d = 4.01R_0$ and Fig. 6 shows the results of the shortest path distribution. The shortest path for all the quadrant pairs in the blue region are LSR, contradicting the proposition 9 in [7].

This proves that the switching function presented in [7]

$$S_{12} = p_{rsr} - p_{rsl} - 2(q_{rsl} - \pi)$$

sometimes doesn't select the actual shorter path between RSR and RSL. The p_{rsr} , p_{rsl} and q_{rsl} lengths of different sections of the path and are defined in [7] and shown in Fig. 7, with the subscript referring to the trajectory type. For an example case shown in Fig. 7, the above switch function

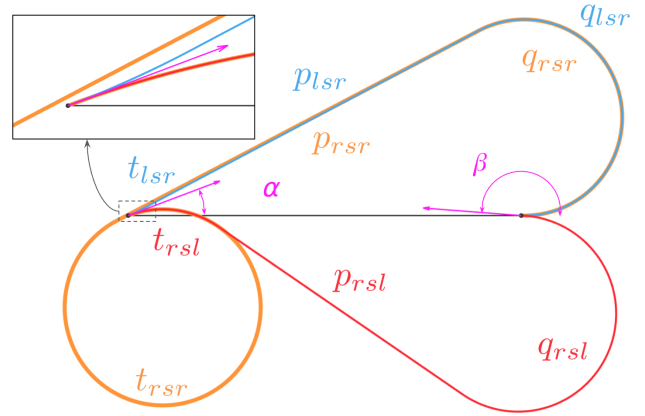


Fig. 7. Plot of RSL, LSR and RSR path for a point $\alpha = 0.36$ and $\beta = 3.111$ in the blue region of 6. Though the length of **LSR** (blue) and **RSL** (red) are very close, the **LSR** path is the shortest among all options after calculation. Area near the starting point is zoomed in for better illustration of the path difference.

provided in [7] would select RSR as the shortest path, but with nearly a whole circle as the first section of its path, RSR is obviously longer than the RSL path.

For our methodology, the decision table is modified so that it can still provide the shortest path for the cases shown above. The modified decision table is provided in Table I with updated entries in $a_{lm} \in \{a_{12}, a_{21}, a_{34}, a_{43}\}$.